



Smoke of extreme Australian bushfires observed in the stratosphere over Punta Arenas, Chile, in January 2020: optical thickness, lidar ratios, and depolarization ratios at 355 and 532 nm

Kevin Ohneiser¹, Albert Ansmann¹, Holger Baars¹, Patric Seifert¹, Boris Barja², Cristofer Jimenez¹, Martin Radenz¹, Audrey Teisseire¹, Athina Floutsi¹, Moritz Haarig¹, Ronny Engelmann¹, Félix Zamorano², Johannes Bühl¹, and Ulla Wandinger¹

¹Leibniz Institute for Tropospheric Research, Leipzig, Germany

²Atmospheric Research Laboratory, University of Magallanes, Punta Arenas, Chile

Correspondence: ohneiser@tropos.de

Abstract.

We present particle optical properties of stratospheric smoke layers observed over Punta Arenas (53.2°S, 70.9°W), Chile, at the southernmost tip of South America in January 2020. The smoke originated from the record-breaking bushfires in Australia. The stratospheric aerosol optical thickness reached values up to 0.7 at 532 nm in mid January 2020. The measured smoke extinction-to-backscatter ratios (lidar ratios) and linear depolarization ratios at 355 and 532 nm wavelength indicate shape, size, and light-absorption properties and are important input parameters in the analysis of spaceborne lidar observations of the CALIPSO and Aeolus missions. They are also of key importance regarding the homogenization of the overall Aeolus (355 nm wavelength) and CALIPSO (532 nm wavelength) smoke data sets and interpretation of the observations with respect to the spread of the smoke particles across the southern hemisphere and decay of the stratospheric perturbation. We found typical values and spectral dependencies of the lidar ratio and linear depolarization ratio for aged stratospheric smoke. At 355 nm, the lidar ratio and depolarization ratio ranged from 53-97 sr and 0.2-0.26, respectively. At 532 nm, the lidar ratios were higher (76-104 sr) and the depolarization ratios were lower with values around 0.15. The found lidar ratio and depolarization ratio values for Australian smoke are in good agreement with respective ones obtained from observations of stratospheric smoke layers over central Europe originating from the record-breaking Canadian wildfires in the summer of 2017. The higher 532 nm lidar ratios, however, indicate stronger absorption by the Australian smoke particles.

1 Introduction

Massive bushfires fueled by high, record-breaking temperatures were raging in southeastern Australia in the summer season of 2019-2020 after months of extreme drought. These were the worst wildfires since decades. More than 150000 km² of land burned until mid of January 2020. The enormous fire activity triggered strong pyrocumulonimbus (pyroCB) convection (Frommel et al., 2003, 2010) in the last days of December 2019 and in January 2020 (NASA, 2020). The pyroCB towers reached heights of 15-16 km and lifted enormous amounts of fire smoke into the upper troposphere and lower stratosphere. Absorption



of sunlight by the black-carbon-containing smoke particles caused warming of the smoke layers and further ascend of the aerosol particles (Boers et al., 2010; de Laat et al., 2012) up to more than 20 km height as observed with the spaceborne lidar CALIOP (Cloud–Aerosol Lidar with Orthogonal Polarization) of the CALIPSO (Cloud–Aerosol Lidar and Infrared Pathfinder Satellite Observation) mission (CALIPSO, 2020). The prevailing westerly winds transported the smoke layers to South America within about 10–20 days. First stratospheric smoke layers were detected with our lidar system over Punta Arenas, Chile, at the southernmost tip of South America in the evening of 5 January 2020, after a travel of around 10000 km. In contrast, enhanced levels of free tropospheric concentrations of Australian fire smoke particles were already observed in the usually rather pristine marine atmosphere over southern Chile since mid November 2019.

The stratospheric aerosol spreads across the southern hemispheric latitudes from about 20–30°S to the south pole within few weeks, in a similar way as observed after injections of fire smoke into the northern hemispheric stratosphere (Fromm et al., 2008; Baars et al., 2019). Stratospheric aerosol perturbations influence radiative transfer, ice cloud formation in the upper troposphere, and chemical processes in the lower stratosphere over months. The smoke enriches the natural soot particle reservoir between 20–30 km (Renard et al., 2008). The height-resolved documentation of this unique event including the decay of the stratospheric perturbation will be mainly based on observations with NASA’s spaceborne lidar CALIOP (Winker et al., 2009; Omar et al., 2009; Khaykin et al., 2018; Kar et al., 2019) and ALADIN (Atmospheric LASer Doppler INSTRUMENT) of the Aeolus mission of the European Space Agency (ESA) (Stoffelen et al., 2005; ESA, 2008; Lux et al., 2020; Witschas et al., 2020; Ansmann et al., 2007; Flamant et al., 2008). However, these spaceborne lidar observations need support by advanced ground-based lidar systems especially regarding measurements of the smoke extinction-to-backscatter ratio (lidar ratio) and depolarization ratio at 355 and 532 nm wavelength. The observations are required as input parameters in the data analysis of the space lidar measurements conducted at different laser wavelengths, namely at 355 nm in the case of Aeolus lidar and 532 nm in the case of CALIPSO lidar. Lidar ratios and depolarization ratios measured simultaneously at both wavelengths are rather useful also with respect to the homogenization of the overall Aeolus–CALIPSO data set of smoke optical properties. Ground-based lidar observations are generally required in the framework of ground truth activities to guarantee high quality of the spaceborne lidar observations (see, e.g., Tesche et al., 2013). Furthermore, such detailed lidar observations of particle optical properties, as presented here, allow us to draw conclusions on the chemical composition (aerosol type), absorption and scattering properties, and size and shape characteristics of the particles (see, e.g., Burton et al., 2012, 2015; Groß et al., 2013). Our Australian smoke observations can thus be regarded as a valuable contribution to the aerosol typing library.

In this rapid communication, we present first Punta Arenas lidar measurements of lidar ratios and depolarization ratios at 355 and 532 nm of the Australian stratospheric bushfire smoke with an advanced polarization Raman lidar (Engelmann et al., 2016; Baars et al., 2016) performed during January 2020. In Sect. 2, the lidar and the data analysis is briefly explained. Section 3 contains the observations. A few concluding remarks are given in Sect. 4.



2 Lidar apparatus and data analysis

The lidar observations at Punta Arenas (53.2°S, 70.9°W, 9 m above sea level, a.s.l.), Chile, were conducted in the framework of the DACAPO-PESO (Dynamics, Aerosol, Cloud And Precipitation Observations in the Pristine Environment of the Southern Ocean, <https://dacapo.tropos.de>) campaign lasting from November 2018 to April 2020. The main goal of DACAPO-PESO is the investigation of aerosol-cloud interaction processes at rather pristine, unpolluted marine environmental conditions. The mobile Leipzig Cloudnet supersite LACROS (Leipzig Aerosol and Cloud Remote Observation System, <http://lacros.rsd.tropos.de/>) (Bühl et al., 2013, 2016) was run continuously at the University of Magallanes (UMAG) at Punta Arenas and covered two summer and one winter season of aerosol and cloud observations. LACROS is equipped with a multiwavelength polarization Raman lidar, a wind Doppler lidar, 35 GHz Doppler cloud radar, ceilometer, disdrometer, and microwave radiometer. In addition, an Aerosol Robotic Network (AERONET) sun photometer (Holben et al., 1998) was operated.

The Polly instrument (*POrtabLle Lidar sYstem*) (Engelmann et al., 2016) is the key instrument of LACROS for aerosol profiling and installed inside a container. This lidar has 13 channels and continuously measures elastically and Raman backscatter signals at the laser wavelengths of 355, 532, and 1064 nm and respective Raman backscattering wavelengths of 387 and 607 nm (nitrogen Raman scattering) and 407 nm (water vapor Raman scattering) (Baars et al., 2016, 2019). These polarization Raman lidar observations permit us to determine height profiles of the particle backscatter coefficient at the laser wavelengths of 355, 532 and 1064 nm wavelength, particle extinction coefficients at 355 and 532 nm, the particle linear depolarization ratio at 355 and 532 nm, and of the water-vapor-to-dry-air mixing ratio by using the Raman lidar return signals of water vapor and nitrogen (Engelmann et al., 2016; Hofer et al., 2017; Dai et al., 2018). The linear depolarization ratio is defined as the cross-polarized-to-co-polarized backscatter ratio. Co and Cr denote the planes of polarization parallel and orthogonal to the plane of linear polarization of the transmitted laser pulses, respectively.

Details of the stratospheric Polly data analysis including an uncertainty discussion is given in the recent publication of Baars et al. (2019) on stratospheric smoke observations in the northern hemisphere. Auxiliary data are required in the lidar data analysis in form of temperature and pressure profiles in order to calculate and correct for Rayleigh backscatter and extinction influences on the measured lidar return signal profiles. As auxiliary meteorological observations we used GDAS1 (Global Data Assimilation System 1) temperature and pressure profiles with 1° horizontal resolution from the National Weather Service's National Centers for Environmental Prediction (GDAS, 2020). We checked the quality and accuracy of the GDAS1 profiles by comparison with respective temperature and pressure profiles measured with radiosonde at Punta Arenas airport (daily launch at 12 UTC). Furthermore, the HYSPLIT model (Hybrid Single Particle Lagrangian Integrated Trajectory Model) (HYSPLIT, 2020; Stein et al., 2015; Rolph et al., 2017) based on GDAS1 reanalysis data was used to calculate 10-20 day backward trajectories.

3 Observations

The year 2019 was Australia's warmest year (Bureau of Meteorology, Australia). Furthermore, the spring of 2019 was the driest of the Bureau of Meteorology's 120 years of rainfall records. These extreme conditions favored strong and long-lasting bush-



fires during the summer months of 2019-2020. Vigorous, deep pyroCB convection evolved over the fire areas and lifted large amounts of smoke to the upper troposphere and lower stratosphere within hours. Predominating westerly winds transported the fire particles eastward towards and across South America. Figure 1 shows the aerosol layering over Punta Arenas on 6, 9, and 10 January 2020. First pronounced fire smoke layers in the stratosphere (above 12 km height above ground level, a.g.l.) were detected on 5 January 2020. Before, Australian smoke crossed the lidar site at tropospheric heights since mid November 2019. An impressive example for tropospheric smoke is shown in Fig. 1a. A pronounced free tropospheric smoke layer between 4 and 10 km height occurred on 6 January 2020. The layer contained many ice clouds, probably a result of heterogeneous ice nucleation on insoluble soot particles which are favorable ice-nucleating particles especially at temperatures below -40°C (Ullrich et al., 2017). On 9 January 2020, an optically dense stratospheric smoke layer crossed the field site (Fig. 1b). The aerosol optical thickness (AOT) partly exceeded 0.2 at 532 nm. The maximum 532 nm AOT of 0.7 was observed on 17 January 2020 as will be discussed below. The measurements taken on 9 January 2020 are discussed in detail in Fig. 3. During the next days smoke layers could be observed over Punta Arenas almost on a daily basis, although low-level liquid-water clouds occasionally inhibited the acquisition of lidar profiles up the stratospheric smoke layers.

The 20-day backward trajectories in Fig. 2 indicate transport of aerosol from the region of Australia towards the southern parts of South America. The trajectories have to be interpreted with caution, the uncertainty is large. The trajectories thus provide a rough view on the general airflow only. As can be seen, air masses obviously started over Australia at heights of 15-16 km and arrived over Punta Arenas at heights of 12-14 km. The trajectories do not include an ascent of the aerosol layers by sunlight absorption and warming of the smoke layers during the long-range transport. As suggested above, we can conclude that aerosol starting in Australia at such high altitudes of 15-16 km must have been lifted to these heights by strong convective activity associated with pyroCB evolution over and downwind the hot fire areas (Fromm et al., 2003, 2010; NASA, 2020).

Figure 3 presents the full set of particle optical properties derived from the Polly measurements on 9 January 2020 (see Fig. 1b). Two-hour mean height profiles of the particle backscatter and extinction coefficients and respective extinction-to-backscatter ratios (lidar ratios) as well as of the particle linear depolarization ratios at 355 and 532 nm are shown. Signal smoothing is applied with window lengths of about 500 m in the case of the backscatter coefficient and depolarization ratio profiles and 2000 m in the case of the extinction coefficient and lidar ratio profiles. The results (especially for 355 nm, strong Rayleigh attenuation) are noisy because the Polly lidar is designed and optimized for tropospheric aerosol observations, but not for monitoring of exceptionally occurring stratospheric aerosol events as mentioned already by Baars et al. (2019). Nevertheless, the layer mean values for the different optical parameters, highlighted as vertical lines in Fig. 3, provide a clear picture of the microphysical and chemical properties of the aged stratospheric smoke particles. As typical for aged smoke, the spectral dependency of the backscatter coefficient is large, whereas the wavelength dependence of the extinction coefficient (for the short wavelength range from 355 to 532 nm) is less pronounced. As a consequence, the lidar ratio is significantly larger at 532 nm than for 355 nm. The measured depolarization ratios are surprisingly high with values around 0.2 (355 nm) and 0.15 (532 nm). However, similar values were observed for stratospheric smoke in the northern hemisphere originating from Canadian wildfires in August 2017 (Haarig et al., 2018; Hu et al., 2019). The reason for the enhanced depolarization ratio values is probably the slightly non-spherical shape of the smoke particles (Yu et al., 2019; Gialli et al., 2019), whereas the



strong spectral slope is caused by the narrow size distribution (Dahlkötter et al., 2014; Haerig et al., 2018) and the absence of a coarse mode (particles with diameters $>1 \mu\text{m}$). These aspects are further discussed below. According to Yu et al. (2019), the Canadian smoke particles consisted of an insoluble black carbon (BC) core that was surrounded by an almost spherical shell of organic material and other atmospheric substances. Most smoke particles were found in the accumulation mode with diameters
5 mostly $<1 \mu\text{m}$. A similar picture of the composition, structure and size distribution obviously holds for Australian smoke.

The findings in Fig. 3 are complemented by the results given in Table 1. Geometrical and optical properties of smoke layers observed on three subsequent days (8-10 January 2020) are summarized. Large lidar ratios of 76-104 sr were observed at 532 nm indicating strongly absorbing BC containing smoke particles. The lidar ratio at 355 nm was about 20 sr lower than the 532 nm lidar ratios on 8 and 9 January. Typical depolarization ratios for stratospheric smoke with values around 0.15 at 532 nm
10 and of 0.2 and larger at 355 nm were determined.

In Fig.4, the similarity between Canadian and Australian smoke lidar and depolarization ratios is highlighted. The slightly higher lidar ratios for Australian smoke indicate stronger absorption by the smoke particles. This is probably related to the different burning material. A large fraction of forest trees are pines and firs in Canada, but eucalyptus trees prevail in Australia. However, also the fire type (smouldering vs flaming) influences the chemical composition of the smoke particles and thus their
15 light-absorption efficiency. High lidar ratios were also observed for wildfire smoke particles originating from central Africa (Tesche et al., 2011) and from South Africa (Giannakaki et al., 2016). The African lidar ratios for 355 and 532 nm were similar which, in turn, is an indication that the measured smoke was relatively fresh (of regional origin), and not aged as observed over Punta Arenas. A review on smoke lidar ratios and depolarization ratios in the troposphere and stratosphere can be found in Haerig et al. (2018).

In contrast to the Polly observations in Punta Arenas, even the depolarization ratio at 1064 nm could be measured at the central European lidar station of Leipzig, Germany, in the case of Canadian smoke (Haerig et al., 2018). The strong wavelength dependence of the depolarization ratio from 355 to 1064 nm and the very low 1064 nm depolarization ratio values are a strong hint that coarse mode smoke particles were absent in the stratosphere. The size distribution showed a well developed accumulation mode as typical for wildfire smoke (Dahlkötter et al., 2014). Gialitaki et al. (2019) modeled the optical properties
25 (depolarization and lidar ratios at 355, 532, and 1064 nm) of the aged non-spherical smoke particles and concluded that the smoke particles were compact and almost spherical in shape.

In Fig.4a, we added the 355 nm lidar ratio (see star symbol) that would be obtained from the Aeolus lidar observation. The ALADIN observations permit the retrieval of backscatter and extinction coefficients and thus of the lidar ratio (Ansmann et al., 2007). The spaceborne lidar transmits circularly polarized laser pulses. Due to the specific receiver configuration of ALADIN,
30 the backscatter signal is however equal to the theoretically possible total backscatter signal (caused by elastic backscattering by air molecules and particles) only when the particle linear depolarization ratio of the smoke particles is zero. In the case of stratospheric smoke showing a depolarization ratio of 0.2, the particle-related backscatter signal measured with ALADIN is a factor of 1.5 lower than the total particle-related backscatter signal at 355 nm. It follows from further mathematical treatments that the corresponding particle lidar ratio is a factor of 1.5 larger than the true one, measured with our Polly instrument. In



conclusion, the knowledge of the 355 nm linear depolarization ratio allows us to correct for this signal loss effect and to derive at the end the true lidar ratio of 53 sr also from the Aeolus lidar observations.

Finally, Fig.5 provides an overview of the stratospheric smoke conditions from 6-20 January 2020 in terms of AOT, layer mean extinction coefficient, lidar ratio and depolarization ratio for 532 nm. The stratospheric aerosol layers occurred mainly
5 between 10 and 20 km height, and showed vertical depths from a few hundreds of meters up to several kilometers. The shown AOT and layer mean extinction values are computed from the particle backscatter coefficients multiplied by a lidar ratio of 80 sr. A peak AOT value of 0.7 at 532 nm was measured from 8:00-9:00 UTC on 17 January 2020, in good agreement with the AERONET photometer measurements at the Punta-Arenas-UMAG and CEILAP-RG sites (AERONET, 2020) on this day (starting at about 10:00 UTC). Note that the photometers underestimate the stratospheric AOT by roughly 30% due to multiple
10 scattering effects as discussed by Ansmann et al. (2018). A similar maximum value of the stratospheric AOT (0.6 in the summer of 2017) was observed with lidar over central Europe for the record-breaking Canadian wildfires (Ansmann et al., 2018). The layer mean extinction values for the Australian smoke were typically between about 20-60 Mm^{-1} , peak values were close to 350 Mm^{-1} on 17 January 2020. According to the few lidar ratios in Fig.5d, strongly absorbing smoke particles prevailed.

The ongoing lidar observations at Punta Arenas showed that the main smoke layer further ascended and reached heights up
15 to 27 km on 28-30 January 2020. The 355 and 532 nm depolarization ratios were close to 0.25 and 0.2, respectively, and the lidar ratios remained high.

4 Conclusion/Outlook

Important input parameters required for a trustworthy CALIPSO and Aeolus lidar data analysis of the stratospheric Australian smoke observations have been presented. Strong perturbations of the stratospheric aerosol conditions with AOT up to 0.7 at
20 532 nm were recorded. The stratospheric smoke lidar ratios and depolarization ratios were found to be similar to the ones observed over Europe in the summer of 2017 during the record-breaking fire season in western Canada. However, Australian smoke showed higher lidar ratios (76-104 sr at 532 nm) which indicates stronger light-absorption.

Significantly enhanced particle linear depolarization ratios of about 0.15 (532 nm) and 0.2-0.26 (at 355 nm) were found mid of January 2020 and point to non-spherical accumulation-mode particles and the absence of coarse-mode particles. The Polly
25 observations are ongoing until the end of the DACAPO-PESO campaign in April 2020 and thus will cover the entire bushfire season and most of the decay phase of the stratospheric perturbation. We will present the entire fire period in terms of the measured smoke optical properties in an extended article.

The record-breaking intense Australian fires also caused a significant increase of the particle concentration in the free troposphere. Clean pristine marine conditions were no longer observable over Punta Arenas since mid November 2019. Regarding
30 our aerosol-cloud-interaction studies in the framework of the DACAPO-PESO campaign, we plan to distinguish and separate time periods with and without smoke pollution from Australia to evaluate the potential impact of smoke on cloud and precipitation evolution in the usually pristine environment of the Southern Ocean.



5 Data availability

LACROS data are accessible through the ACTRIS data portal <http://actris.nilu.no/>. The long-term Polly lidar level-0 data are plotted online at polly.tropos.de, raw data are available at TROPOS upon request (<http://polly.rsd.tropos.de/>). All the analysis products are available at TROPOS upon request (info@tropos.de). All AERONET data used in this work can be accessed through the AERONET home page at <https://aeronet.gsfc.nasa.gov/>. GDAS1 data is available via the ARL webpage <https://www.ready.noaa.gov/gdas1.php>.

6 Author contributions

The paper was written by KO and AA. The data analysis was performed by KO supported by HB, AA, AF, MH, and UW. All other co-authors are involved in the DACAPO-PESO campaign and took care of all measurements during several 4-week travels.

7 Competing interests

The authors declare that they have no conflict of interest.

8 Financial support

TROPOS is involved in the Calibration/Validation (Cal/Val) activities of the Aeolus space mission in the frame of the German initiative EVAA (Experimental Validation and Assimilation of Aeolus observations) funded by the German Federal Ministry for Economic Affairs and Energy (BMWi) under grant no. (FKZ) 50EE1721C. The authors acknowledge also support through the European Research Infrastructure for the observation of Aerosol, Clouds and Trace Gases ACTRIS under grant agreement no. 654109 and 739530 from the European Union's Horizon 2020 research and innovation programme. We thank AERONET-Europe for providing an excellent calibration service. AERONET-Europe is part of the ACTRIS project. The DACAPO-PESO observations are partly funded by the German Science Foundation (DFG) project PICNICC with project number 408008112.

Acknowledgements. We thank AERONET for their continuous efforts in providing high-quality measurements and products. Aerosol sources apportionment analysis has been supported by air mass transport computation with the NOAA (National Oceanic and Atmospheric Administration) HYSPLIT (HYbrid Single-Particle Lagrangian Integrated Trajectory) model using GDAS meteorological data.



References

- AERONET: AERONET aerosol data base, available at: <http://aeronet.gsfc.nasa.gov/>, last access: 20 January, 2020.
- Ansmann, A., Wandinger, U., Le Rille, O., Lajas, D., and Straume, A.: Particle backscatter and extinction profiling with the spaceborne high-spectral-resolution Doppler lidar ALADIN: methodology and simulations, *Appl. Opt.*, 46, 6606–6622, 2007
- 5 Ansmann, A., Baars, H., Chudnovsky, A., Mattis, I., Veselovskii, I., Haarig, M., Seifert, P., Engelmann, R., and Wandinger, U.: Extreme levels of Canadian wildfire smoke in the stratosphere over central Europe on 21–22 August 2017, *Atmos. Chem. Phys.*, 18, 11831–11845, <https://doi.org/10.5194/acp-18-11831-2018>, 2018.
- Baars, H., Kanitz, T., Engelmann, R., Althausen, D., Heese, B., Komppula, M., Preißler, J., Tesche, M., Ansmann, A., Wandinger, U., Lim, J.-H., Ahn, J. Y., Stachlewska, I. S., Amiridis, V., Marinou, E., Seifert, P., Hofer, J., Skupin, A., Schneider, F., Bohlmann, S., Foth, A.,
- 10 Bley, S., Pfüller, A., Giannakaki, E., Lihavainen, H., Viisanen, Y., Hooda, R. K., Pereira, S. N., Bortoli, D., Wagner, F., Mattis, I., Janicka, L., Markowicz, K. M., Achtert, P., Artaxo, P., Pauliquevis, T., Souza, R. A. F., Sharma, V. P., van Zyl, P. G., Beukes, J. P., Sun, J., Rohwer, E. G., Deng, R., Mamouri, R.-E., and Zamorano, F.: An overview of the first decade of PollyNET: an emerging network of automated Raman-polarization lidars for continuous aerosol profiling, *Atmos. Chem. Phys.*, 16, 5111–5137, doi:10.5194/acp-16-5111-2016, 2016.
- Baars, H., Ansmann, A., Ohneiser, K., Haarig, M., Engelmann, R., Althausen, D., Hanssen, I., Gausa, M., Pietruczuk, A., Szkop, A., Stachlewska, I. S., Wang, D., Reichardt, J., Skupin, A., Mattis, I., Trickl, T., Vogelmann, H., Navas-Guzmán, F., Haefele, A., Acheson, K.,
- 15 Ruth, A. A., Tatarov, B., Müller, D., Hu, Q., Podvin, T., Goloub, P., Veselovskii, I., Pietras, C., Haeffelin, M., Fréville, P., Sicard, M., Comerón, A., Fernández García, A. J., Molero Menéndez, F., Córdoba-Jabonero, C., Guerrero-Rascado, J. L., Alados-Arboledas, L., Bortoli, D., Costa, M. J., Dionisi, D., Liberti, G. L., Wang, X., Sannino, A., Papagiannopoulos, N., Boselli, A., Mona, L., D’Amico, G., Romano, S., Perrone, M. R., Belegante, L., Nicolae, D., Grigorov, I., Gialitaki, A., Amiridis, V., Soupiona, O., Papayannis, A.,
- 20 Mamouri, R.-E., Nisantzi, A., Heese, B., Hofer, J., Schechner, Y. Y., Wandinger, U., and Pappalardo, G.: The unprecedented 2017–2018 stratospheric smoke event: decay phase and aerosol properties observed with the EARLINET, *Atmos. Chem. Phys.*, 19, 15183–15198, <https://doi.org/10.5194/acp-19-15183-2019>, 2019.
- Boers, R., de Laat, A. T., Stein Zweers, D. C., and Dirksen, R. J.: Lifting potential of solar-heated aerosol layers, *Geophys. Res. Lett.*, 37, L24802, doi:10.1029/2010GL045171, 2010.
- 25 Bühl, J., Seifert, P., Wandinger, U., Baars, H., Kanitz, T., Schmidt, J., Myagkov, A., Engelmann, R., Skupin, A., Heese, B., Klepel, A., Althausen, D., and Ansmann, A.: LACROS: the Leipzig Aerosol and Cloud Remote Observations System, *Proc. SPIE* 8890, 889002, <https://doi.org/10.1117/12.2030911>, 2013.
- Bühl, J., Seifert, P., Myagkov, A., and Ansmann, A.: Measuring ice- and liquid-water properties in mixed-phase cloud layers at the Leipzig Cloudnet station, *Atmos. Chem. Phys.*, 16, 10609–10620, <https://doi.org/10.5194/acp-16-10609-2016>, 2016.
- 30 Burton, S. P., Ferrare, R. A., Hostetler, C. A., Hair, J. W., Rogers, R. R., Obland, M. D., Butler, C. F., Cook, A. L., Harper, D. B., and Froyd, K. D.: Aerosol classification using airborne High Spectral Resolution Lidar measurements – methodology and examples, *Atmos. Meas. Tech.*, 5, 73–98, <https://doi.org/10.5194/amt-5-73-2012>, 2012.
- Burton, S. P., Hair, J. W., Kahnert, M., Ferrare, R. A., Hostetler, C. A., Cook, A. L., Harper, D. B., Berkoff, T. A., Seaman, S. T., Collins, J. E., Fenn, M. A., and Rogers, R. R.: Observations of the spectral dependence of linear particle depolarization ratio of aerosols using NASA
- 35 Langley airborne High Spectral Resolution Lidar, *Atmos. Chem. Phys.*, 15, 13453–13473, doi:10.5194/acp-15-13453-2015, 2015.
- CALIPSO: CALIPSO lidar data base, available at: <https://www-calipso.larc.nasa.gov/products/lidar>, last access: 20 January 2020.



- Dahlkötter, F., Gysel, M., Sauer, D., Minikin, A., Baumann, R., Seifert, P., Ansmann, A., Fromm, M., Voigt, C., and Weinzierl, B.: The Pagami Creek smoke plume after long-range transport to the upper troposphere over Europe – aerosol properties and black carbon mixing state, *Atmos. Chem. Phys.*, 14, 6111–6137, <https://doi.org/10.5194/acp-14-6111-2014>, 2014.
- Dai, G., Althausen, D., Hofer, J., Engelmann, R., Seifert, P., Bühl, J., Mamouri, R.-E., Wu, S., and Ansmann, A.: Calibration of Raman lidar water vapor profiles by means of AERONET photometer observations and GDAS meteorological data, *Atmos. Meas. Tech.*, 11, 2735–2748, <https://doi.org/10.5194/amt-11-2735-2018>, 2018.
- de Laat, A. T. J., Stein Zweers, D. C., Boers, R., and Tuinder, O. N. E.: A solar escalator: Observational evidence of the self-lifting of smoke and aerosols by absorption of solar radiation in the February 2009 Australian Black Saturday plume, *J. Geophys. Res.*, 117, D04204, doi:10.1029/2011JD017016, 2012.
- Engelmann, R., Kanitz, T., Baars, H., Heese, B., Althausen, D., Skupin, A., Wandinger, U., Komppula, M., Stachlewska, I. S., Amiridis, V., Marinou, E., Mattis, I., Linné, H., and Ansmann, A.: The automated multiwavelength Raman polarization and water-vapor lidar PollyXT: the neXT generation, *Atmos. Meas. Tech.*, 9, 1767–1784, doi:10.5194/amt-9-1767-2016, 2016.
- ESA: European Space Agency, ADM-Aeolus Science Report, ESA SP-1311, available at: http://esamultimedia.esa.int/docs/730SP-1311__ADM-Aeolus_a__FINA__low-res.pdf, 2008.
- Flamant, P., Cuesta, J., Denneulin, M. L., Dabas, A., and Huber, D.: ADM-Aeolus retrieval algorithms for aerosol and cloud products, *Tellus A*, 60, 273–288, doi:10.1111/j.1600-0870.2007.00287.x, 2008.
- Fromm, M. D., and Servranckx, R.: Transport of forest fire smoke above the tropopause by supercell convection, *Geophys. Res. Lett.*, 30, 1542, doi:10.1029/2002GL016820, 2003.
- Fromm, M., Shettle, E. P., Fricke, K. H., Ritter, C., Trickl, T., Giehl, H., Gerding, M., Barnes, J. E., O’Neill, M., Massie, S. T., Blum, U., McDermid, I. S., Leblanc, T., and Deshler, T.: Stratospheric impact of the Chisholm pyrocumulonimbus eruption: 2. Vertical profile perspective, *J. Geophys. Res.*, 113, D08203, doi:10.1029/2007JD009147, 2008.
- Fromm, M., Lindsey, D. T., Servranckx, R., Yue, G., Trickl, T., Sica, R., Doucet, P., and Godin-Beekmann, S. E.: The untold story of pyrocumulonimbus, *B. Am. Meteorol. Soc.*, 91, 1193–1209, doi:10.1175/2010bams3004.1, 2010.
- GDAS: Global Data Assimilation System, meteorological data base, available at: <https://www.ready.noaa.gov/gdas1.php>, last access: 20 January, 2020.
- Gialitaki, A., Tsekeri, A., Amiridis, V., Ceolato, R., Paulien, L., Proestakis, E., Marinou, E., Haarig, M., Baars, H., and Balis, D.: Is near-spherical shape the "new black" for smoke?, in: Proceedings of the 29th International Laser Radar Conference (ILRC), 24–28 June 2019, Hefei, Anhui, China, pages = S2-114–S2-117, 2019.
- Giannakaki, E., van Zyl, P. G., Müller, D., Balis, D., and Komppula, M.: Optical and microphysical characterization of aerosol layers over South Africa by means of multi-wavelength depolarization and Raman lidar measurements, *Atmos. Chem. Phys.*, 16, 8109–8123, <https://doi.org/10.5194/acp-16-8109-2016>, 2016.
- Groß, S., Esselborn, M., Weinzierl, B., Wirth, M., Fix, A., and Petzold, A.: Aerosol classification by airborne high spectral resolution lidar observations, *Atmos. Chem. Phys.*, 13, 2487–2505, doi:10.5194/acp-13-2487-2013, 2013.
- Haarig, M., Ansmann, A., Baars, H., Jimenez, C., Veselovskii, I., Engelmann, R., and Althausen, D.: Depolarization and lidar ratios at 355, 532, and 1064 nm and microphysical properties of aged tropospheric and stratospheric Canadian wildfire smoke, *Atmos. Chem. Phys.*, 18, 11847–11861, <https://doi.org/10.5194/acp-18-11847-2018>, 2018.
- Hofer, J., Althausen, D., Abdullaev, S. F., Makhmudov, A. N., Nazarov, B. I., Schettler, G., Engelmann, R., Baars, H., Fomba, K. W., Müller, K., Heinold, B., Kandler, K., and Ansmann, A.: Long-term profiling of mineral dust and pollution aerosol with multiwave-



- length polarization Raman lidar at the Central Asian site of Dushanbe, Tajikistan: case studies, *Atmos. Chem. Phys.*, 17, 14559–14577, <https://doi.org/10.5194/acp-17-14559-2017>, 2017.
- Holben, B. N., Eck, T. F., Slutsker, I., Tanré, D., Buis, J. P., Setzer, A., Vermote, E., Reagan, J. A., Kaufman, Y. J., Nakajima, T., Lavenu, F., Jankowiak, I., and Smirnov, A.: AERONET – a federated instrument network and data archive for aerosol characterization, *Remote Sens. Environ.*, 66, 1–16, 1998.
- Hu, Q., Goloub, P., Veselovskii, I., Bravo-Aranda, J.-A., Popovici, I. E., Podvin, T., Haeffelin, M., Lopatin, A., Dubovik, O., Pietras, C., Huang, X., Torres, B., and Chen, C.: Long-range-transported Canadian smoke plumes in the lower stratosphere over northern France, *Atmos. Chem. Phys.*, 19, 1173–1193, <https://doi.org/10.5194/acp-19-1173-2019>, 2019.
- HYSPLIT: HYbrid Single-Particle Lagrangian Integrated Trajectory model, backward trajectory calculation tool, available at: http://ready.arl.noaa.gov/HYSPLIT_traj.php, last access: 20 January, 2020.
- Kar, J., Lee, K.-P., Vaughan, M. A., Tackett, J. L., Trepte, C. R., Winker, D. M., Lucker, P. L., and Getzewich, B. J.: CALIPSO level 3 stratospheric aerosol profile product: version 1.00 algorithm description and initial assessment, *Atmos. Meas. Tech.*, 12, 6173–6191, <https://doi.org/10.5194/amt-12-6173-2019>, 2019.
- Khaykin, S. M., Godin-Beekmann, S., Hauchecorne, A., Pelon, J., Ravetta, F., and Keckut, P.: Stratospheric smoke with unprecedentedly high backscatter observed by lidars above southern France, *Geophys. Res. Lett.*, 45, <https://doi.org/10.1002/2017GL076763>, 2018.
- Lux, O., Lemmerz, C., Weiler, F., Marksteiner, U., Witschas, B., Rahm, S., Geiss, A., and Reitebuch, O.: Intercomparison of wind observations from ESA’s satellite mission Aeolus and the ALADIN Airborne Demonstrator, *Atmos. Meas. Tech. Discuss.*, <https://doi.org/10.5194/amt-2019-431>, in review, 2020.
- NASA: NASA, Earth Observatory, 11 January 2020: explosive fire activity in Australia, report on Australian bushfires, available at: <https://earthobservatory.nasa.gov/images/146125/explosive-fire-activity-in-australia?src=eoaiotdlain>, last access: 20 January 2020.
- Omar, A. H., Winker, D. M., Vaughan, M. A., Hu, Y., Trepte, C. R., Ferrare, R. A., Lee, K. P., Hostetler, C. A., Kittaka, C., Rogers, R. R., and Kuehn, R. E.: The CALIPSO Automated Aerosol Classification and Lidar Ratio Selection Algorithm, *J. Atmos. Ocean. Tech.*, 26, 1994–2014, <https://doi.org/10.1175/2009JTECHA1231.1>, 2009.
- Renard, J.-B., Brogniez, C., Berthet, G., Bourgeois, Q., Gaubicher, B., Chartier, M., Balois, J.-Y., Verwaerde, C., Auriol, F., Francois, P., Daugeron, D., and Engrand, C.: Vertical distribution of the different types of aerosols in the stratosphere: Detection of solid particles and analysis of their spatial variability, *J. Geophys. Res.*, 113, D21303, doi:10.1029/2008JD010150, 2008.
- Rolph, G., Stein, A., and Stunder, B.: Real-time Environmental Applications and Display sYstem: READY. *Environmental Modelling & Software*, 95, 210–228, <https://doi.org/10.1016/j.envsoft.2017.06.025>, 2017.
- Siddaway, J. M., and Petelina, S. V.: Transport and evolution of the 2009 Australian Black Saturday bushfire smoke in the lower stratosphere observed by OSIRIS on Odin, *J. Geophys. Res.*, 116, D06203, doi: 10.1029/2010JD015162, 2011.
- Stein, A.F., Draxler, R.R., Rolph, G.D., Stunder, B.J.B., Cohen, M.D., and Ngan, F.: NOAA’s HYSPLIT atmospheric transport and dispersion modeling system, *Bull. Amer. Meteor. Soc.*, 96, 2059–2077, <http://dx.doi.org/10.1175/BAMS-D-14-00110.1>, 2015
- Stoffelen, A., Pailleux, J., Källén, E., Vaughan, J. M., Isaksen, I., Flamant, P., Wergen, W., Andersson, E., Schyberg, H., Culoma, A., Meynart, R., Endemann, M., and Ingmann, P.: The atmospheric dynamics mission for global wind field measurement, *Bulletin of the American Meteorological Society*, 86, 73–88, <https://doi.org/10.1175/BAMS-86-1-73>, 2005.
- Tesche, M., Müller, D., Groß, S., Ansmann, A., Althausen, D., Freudenthaler, V., Weinzierl, B., Veira, A., and Petzold, A.: Optical and microphysical properties of smoke over Cape Verde inferred from multiwavelength lidar measurements. *Tellus B*, 63, 677–694. doi:10.1111/j.1600-0889.2011.00549.x, 2011.



- Tesche, M., Wandinger, U., Ansmann, A., Althausen, D., Müller, D., and Omar, A. H.: Ground-based validation of CALIPSO observations of dust and smoke in the Cape Verde region, *J. Geophys. Res. Atmos.*, 118, 2889–2902–, doi:10.1002/jgrd.50248, 2013.
- Ullrich, R., Hoose, C., Möhler, O., Niemand, M., Wagner, R., Höhler, K., Hiranuma, N., Saathoff, H., and Leisner, T.: A new ice nucleation active site parameterization for desert dust and soot, *J. Atmos. Sci.*, 74, 699–717, 2017.
- 5 Winker, D. M., Vaughna, M. A., Omar, A., Hu, Y., Powell, K. A., Liu, Z., Hunt, W. H., and Young, S. A.: Overview of the CALIPSO mission and CALIOP data processing algorithms, *J. Atmos. Oceanic. Techn.*, 26, 2310–2323, doi:10.1175/2009JTECHA1281.1, 2009.
- Witschas, B., Lemmerz, C., Geiß, A., Lux, O., Marksteiner, U., Rahm, S., Reitebuch, O., and Weiler, F.: First validation of Aeolus wind observations by airborne Doppler Wind Lidar measurements, *Atmos. Meas. Tech. Discuss.*, <https://doi.org/10.5194/amt-2019-432>, in review, 2020.
- 10 Yu, P., Toon, O. B., Bardeen, C. G., Zhu, Y., Rosenlof, K. H., Portmann, R. W., Thornberry, T. D., Gao, R.-S., Davis, S. M., Wolf, E. T., de Gouw, J., Peterson, D. A., Fromm, M. D., and Robock, A.: Black carbon lofts wildfire smoke high into the stratosphere to form a persistent plume, *Science*, 365, 587–590, doi: 10.1126/science.aax1748, 2019.

Table 1. Smoke layer mean values of lidar ratios (LR) and depolarization ratios (DR) simultaneously measured at 355 and 532 nm on three subsequent days in January 2020. Tropopause heights (TPH), layer base heights (LBH), geometrical depths (LGD), and AOTs of the stratospheric smoke layers are given in addition. Wavelength (in nm) is indicated in parentheses. The uncertainty in the layer mean values is mainly caused by signal noise estimated to be about 10% (DR, 532 nm), 20% (LR, 532 nm, DR, 355 nm), and 30% (LR, 355 nm).

Date	TPH [km]	LBH [km]	LGD [km]	AOT(355)	AOT(532)	LR(355) [sr]	LR(532) [sr]	DR(355)	DR(532)
8 Jan 2020, 04:30-06:30 UTC	8.8	13.0	1.6	0.07	0.05	83	102	0.23	0.14
9 Jan 2020, 03:56-05:40 UTC	8.9	12.8	2.9	0.19	0.15	53	76	0.20	0.14
10 Jan 2020, 02:25-04:20 UTC	10.2	16.3	2.7	0.21	0.14	97	104	0.26	0.15

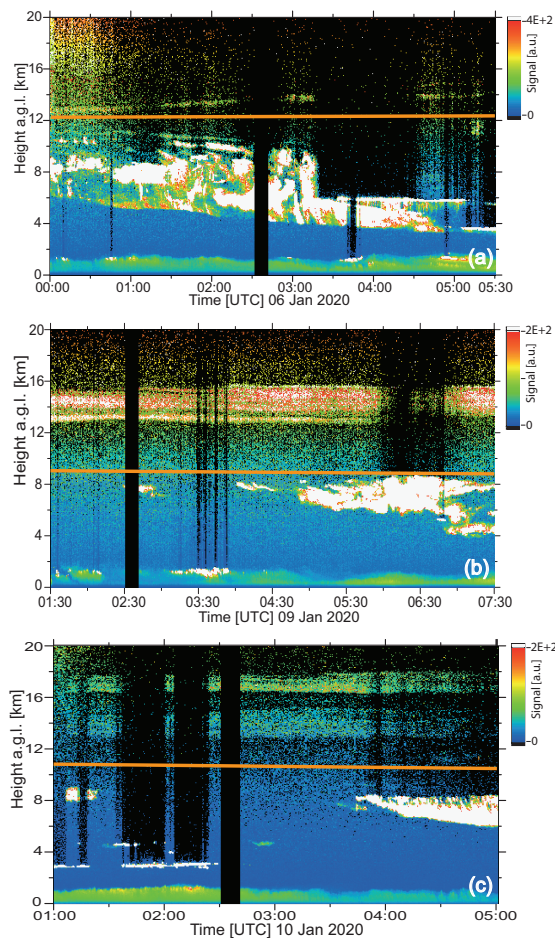


Figure 1. Australian bushfire smoke in the stratosphere at heights (a.g.l.) from 12 – 18 km over Punta Arenas (53.2°S, 70.9°W, 9 m a.s.l.), Chile, 10000 km downwind of the Australian fire areas. The Polly lidar observations were performed in the nights of (a) 6 January, (b) 9 January, and (c) 10 January 2020. The uncalibrated attenuated backscatter coefficient (range-corrected signal) at 1064 nm is shown. The tropopause height according to the Punta Arenas radiosonde (launched at 12:00 UTC, 08:00 local time) is given as orange horizontal line. Black, column-like filaments above cloud layers (shown as white areas) indicate strong laser pulse attenuation. The large, well-defined black columns (from surface to 20 km) indicate periods of automated depolarization calibration. White areas above 4 km height mostly indicate ice clouds. Strong ice-cloud formation occurred in the smoke layer between 4 km and 10.5 km on 6 January 2020, probably triggered by the presence of the high concentration of ice-nucleating smoke particles.

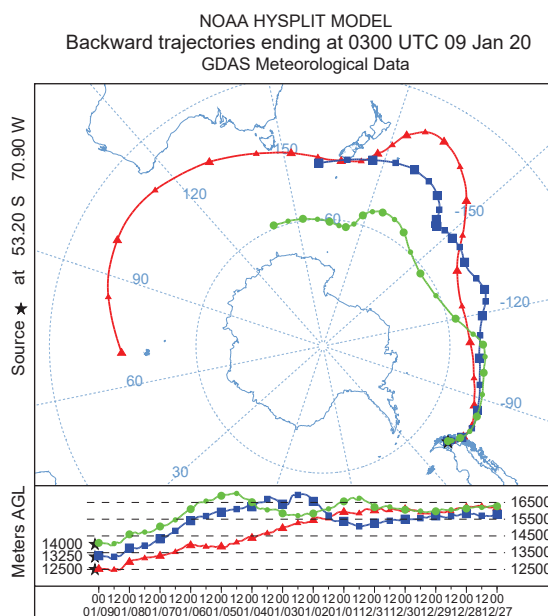


Figure 2. 20-day backward trajectories (Stein et al., 2015; HYSPLIT, 2020) arriving at Punta Arenas on 9 January 2020, 03:00 UTC at 12500 m (red), 13250 m (blue), and 14000 m height (green). Only these trajectories from 12.5–14 km height indicated smoke transport from Australia to South America. However, these trajectories were at great height over the Tasmanian and New Zealand region. This implies that the smoke must have reached these high altitudes around 15–16 km before the eastward transport began. Strong pyroCB convection may have lift the smoke to these high altitudes close to the Australian continent. The further ascend of the smoke layers by absorption of sunlight and warming of the air mass needs to be considered when comparing the 12.5 to 14 km trajectories with the observed smoke layer heights from 13–16 km in Figs. 1b and 3.

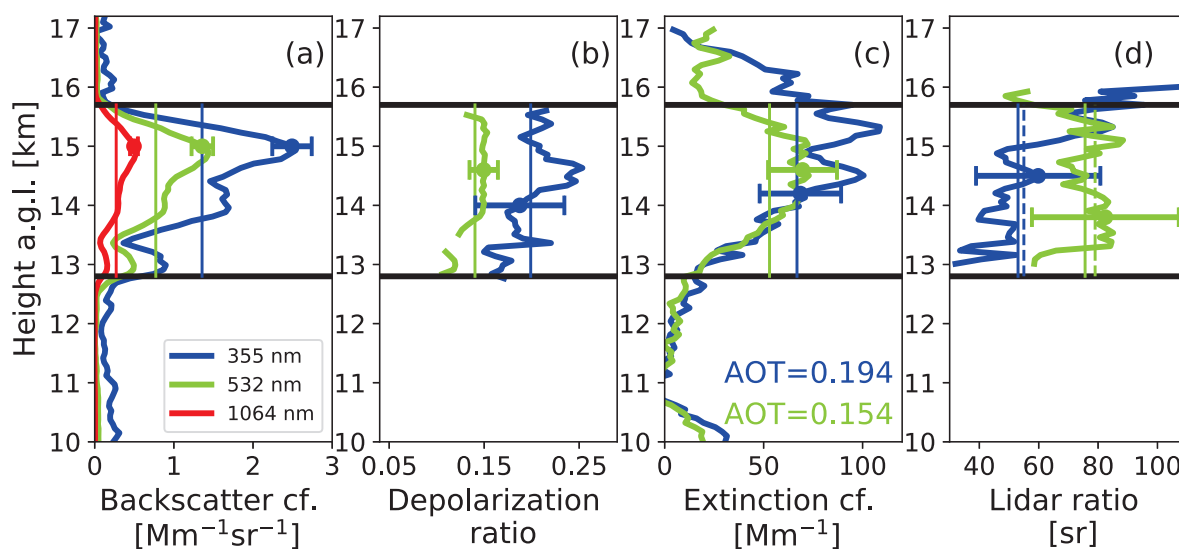


Figure 3. Two-hour mean profiles of smoke optical properties measured in the stratospheric smoke layer. Base and top height of the layer are indicated by black horizontal lines. The Polly measurement was performed on 9 January, 03:56-05:40 UTC (see Fig. 1b): (a) particle backscatter coefficient at three wavelengths, (b) particle linear depolarization ratio, (c) extinction coefficient and AOT, and (d) extinction-to-backscatter ratio (lidar ratio). The backscatter coefficients were calibrated in a thin cirrus layer between 6-8 km height assuming wavelength-independent cirrus backscattering. Colored vertical lines from layer base to top indicate layer mean values. Dashed vertical lines (in d) show column lidar ratios, i.e., the ratio of AOT to column backscatter. Error bars show the estimated uncertainties.

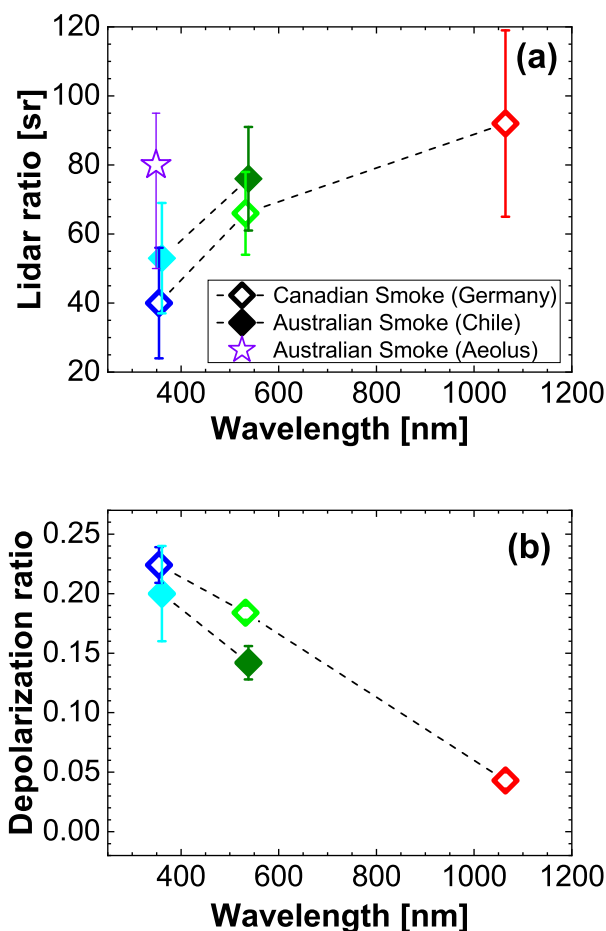


Figure 4. Comparison of the spectral dependence of smoke layer mean values of (a) the particle lidar ratio and (b) the particle linear depolarization ratio measured in Canadian smoke in the stratosphere over Leipzig, Germany, on 22 August 2017 (open symbols) and in Australian smoke in the stratosphere over Punta Arenas, Chile, on 9 January 2020 in Australian bushfire smoke (closed symbols). Similar spectral dependencies for the Canadian and Australian smoke particles are found. Higher lidar ratios for Australian smoke indicate more absorbing particles. Australian forests mainly consists of eucalyptus trees, whereas western Canadian tree types are predominantly pine, fir, aspen, and cedar. Similar depolarization ratio values point to similar shape and size characteristics of Canadian and Australian smoke after long range transport at stratospheric heights. Vertical bars show the retrieval uncertainty. The spaceborne Aeolus lidar (operated at 355 nm) would observe an apparent lidar ratio of more 80 sr (star in a) instead of the true value of 53 sr (see text for more explanations).

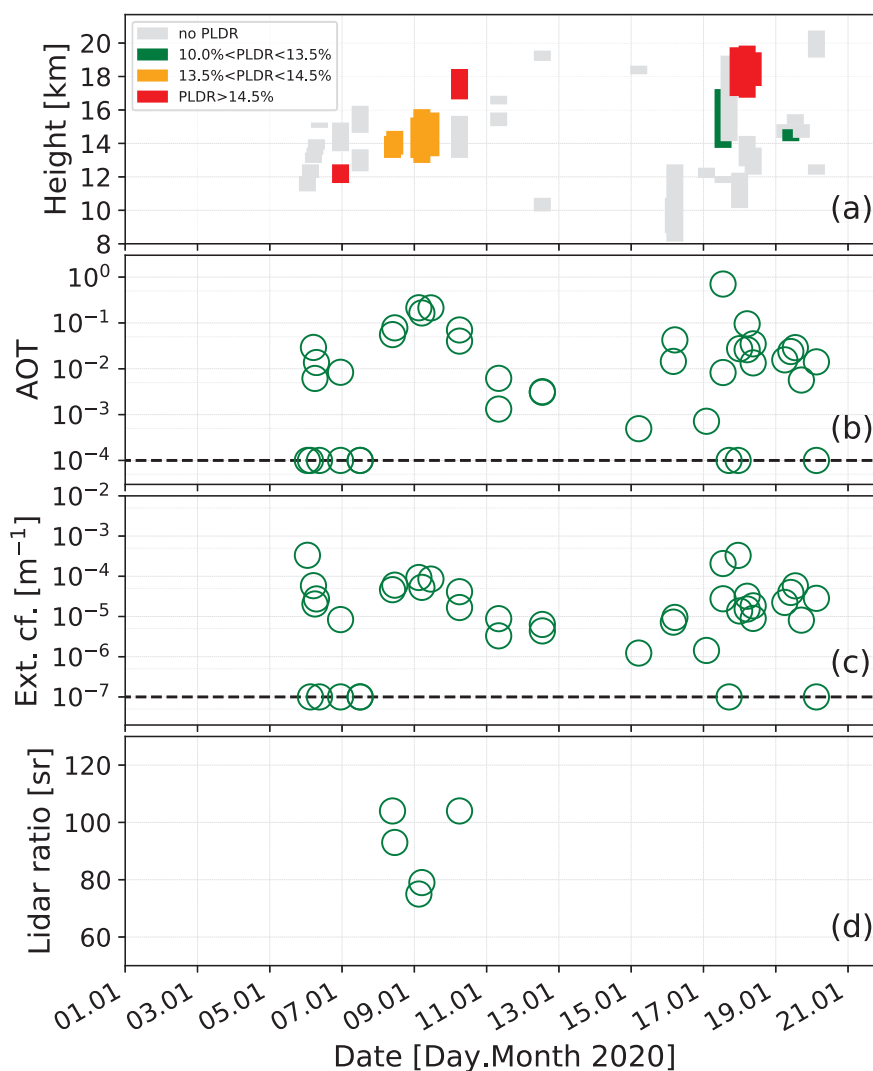


Figure 5. (a) Overview of Polly observations of stratospheric smoke layers (from base to top) from 6-20 January 2020. The color of the layer indicates the layer mean particle linear depolarization ratio (PLDR). If no trustworthy PLDR solution could be obtained, the layers are grey. (b) 532 nm AOT of each detected layer (shown in a), calculated from the backscatter coefficient (from base to top) multiplied by a lidar ratio of 80 sr, (c) corresponding layer mean particle extinction coefficient (AOT in b divided by the geometrical depth in a), and (d) layer mean 532 nm lidar ratio obtained from the nighttime Raman lidar application.